Appl. Phys. A 76, 665–671 (2003)
DOI: 10.1007/s00339-002-2008-1

Applied Physics A
Materials Science & Processing

W. KUCH

Layer-resolved microscopy of magnetic domains in multi-layered systems

Max-Planck-Institut für Mikrostrukturphysik, Weinberg 2, 06120 Halle, Germany

Received: 22 August 2002/Accepted: 2 October 2002
Published online: 5 February 2003 • **© Springer-Verlag 2003**

ABSTRACT Photoelectron emission microscopy in connection with magnetic circular dichroism in soft X-ray absorption can be used for the microscopic imaging of magnetic domains in layered thin film structures consisting of several magnetic layers. Due to the element-selectivity of the method, the different magnetic layers in such a structure can be imaged separately, provided that they contain different elements. This has been applied for the investigation of Co/Cu/Ni trilayers, epitaxially grown on Cu (001). The magnetic coupling between the Co and Ni layers can be directly visualized from comparing layer-resolved magnetic domain images of both layers. As a consequence of the competition between the anisotropy energies of the two magnetic layers and the magnetic coupling energy, spin-reorientation transitions between collinear and non-collinear magnetic configurations are observed. Apart from this globally observable magnetic interlayer coupling a micromagnetic coupling mechanism is also evident from the layer-resolved domain images. It is caused by magnetostatic interaction of local stray fields from domain walls.

PACS 75.70.Kw; 75.70.-i

1 Introduction

Basic and applied research in the field of magnetic thin films have experienced an enormous increase in attention during the last decade. One of the main driving forces behind this progress was the commercial application of giant magnetoresistive effects in sensors and in hard disk read heads [1]. The prospect of assembling magnetic random access memory devices from nano-sized magnetoresistive elements that do not depend on a continuous power supply [2] is further fueling the activity in that field. Many other new and exciting phenomena as spin-polarized tunnelling [3], spin-torque transfer [6, 7], or the injection of spin-polarized electrons into semiconductors [4, 5] have lead to the vision of integrating magnetism into electronic devices in the so-called "spintronics", so that we make use of not only the electron charge as in conventional semiconductor electronics, but also the spin [8–10].

✉ Fax: +49-345/5511-223, E-mail: kuch@mpi-halle.de

All of the above mentioned effects have in common that the structures in which they are observed contain two or more magnetic layers within a multi-layered thin film structure, and that the magnetization of these layers has to be controlled independently. Since these samples are often laterally structured or confined, micromagnetic effects are becoming increasingly important. Apart from electronic transport properties, the understanding and the control of the magnetic coupling between different magnetic layers, also considering micromagnetic effects, is thus a major issue. Its fundamental investigation requires a method that is not only capable of probing the magnetic properties of each magnetic layer separately, but also provides the necessary lateral resolution. Photoelectron emission microscopy (PEEM) in connection with X-ray magnetic circular dichroism (XMCD) in absorption is such a method which has already proven its versatility for the imaging of magnetic domains [11–15].

In XMCD, the absorption of circularly polarized X-rays at elemental absorption edges leads to the excitation of core electrons into the unoccupied valence states just above the Fermi edge. These transitions are spin-polarized due to the absorption of a spin-polarized photon [16]. The relative sign of this spin-polarization with respect to the spin-polarization of the exchange split unoccupied part of the valence band structure determines the absorption cross section [17]. It consequently depends on the relative orientation of the helicity vector of the exciting X-rays and the magnetization direction in the sample. Since elemental absorption edges are excited, this information is obtained element-selectively.

An example is given in Fig. 1. It shows the absorption cross section of a Co/Cu/Ni trilayer as a function of the X-ray photon energy for the two helicities of circularly polarized X-rays. Two pairs of peaks are recognized, which correspond to absorption at the Co L_3 (778 eV) and L_2 edges (793 eV), and at the Ni L_3 (851 eV) and L_2 edges (868 eV). The magnetic dichroism shows up as non-vanishing difference between the two spectra at these absorption peaks. By tuning the photon energy to the Co L_3 edge, information about the magnetization of the Co layer can be obtained; if the photon energy is tuned to the Ni L_3 edge, the difference between the two curves for opposite helicity contains information about the magnetism of the Ni layer. In the example of Fig. 1, comparison of this difference at the Co and Ni absorption edges reveals

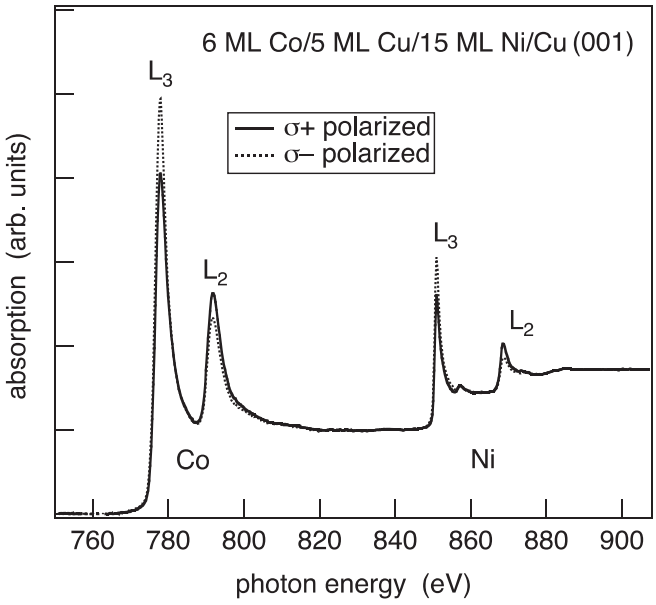

FIGURE 1 Absorption of circularly polarized X-rays as a function of photon energy at a remanently magnetized 6 ML Co/5 ML Cu/15 ML Ni trilayer on Cu (001). Absorption for positive (negative) helicity is shown as a *solid* (*dotted*) line. Absorption maxima are recognized corresponding to the Co and Ni $L_{2,3}$ edges. X-ray magnetic circular dichroism (XMCD) is manifest as a non-vanishing difference between the two spectra at these absorption peaks

that the magnetization directions of both layers, projected on the light incidence direction, have the same sign.

In Fig. 1 the sample current has been recorded as a measure of the X-ray absorption, which is the so-called "total yield" measurement of absorption. It has the advantage of a moderate surface or interface sensitivity, and allows one to study films on top of arbitrarily thick substrates including single crystals. To add lateral resolution to such a total yield XMCD measurement requires the local detection of the current of emitted electrons. Figure 2 schematically explains how this can be achieved with a PEEM. It shows in panel (a) a microstructured sample consisting of four domains, magnetized in a so-called Landau pattern as indicated by the small arrows, which avoids energetically unfavorable magnetic stray fields outside the sample. The local absorption of circularly polarized X-rays at the respective absorption edge will depend on the local magnetization direction, and will differ depending on whether the magnetization in the domains is parallel, antiparallel, or perpendicular to the light incidence direction, as sketched by the width of the curved arrows. A magnified image of the local electron intensity, which is a measure of the absorbed X-ray intensity, will contain the information about the local projection of the magnetization onto the light propagation direction.

Such a magnified image of the local electron intensity can be provided by the PEEM, which is schematically shown in Fig. 2b. It consists of a set of electrostatic lenses on a straight axis. The objective lens creates an intermediate image of the sample surface at the position of the field aperture. This aperture can be used to limit the field of view or to avoid stray electrons. Another aperture, the contrast aperture in the back-focal plane of the objective lens, limits the accepted range of electron emission angles, which is necessary to improve the lateral resolution [18]. An octupolar arrangement of deflection plates serves as stigmator and/or deflector, and can be used for the correction of astigmatism and alignment of the optical axis in any rotational direction. The image is magnified by a two-stage projective lens system, intensified by a double multichannel plate, and recorded off a fluorescent screen by a Peltier-cooled charge coupled device camera outside the vacuum chamber.

In this contribution the use of this XMCD-PEEM technique for the layer-resolved imaging of magnetic domains in coupled Co/Cu/Ni trilayers, epitaxially grown on Cu (001), is demonstrated. Comparison of the Ni and Co domain images directly visualizes the local magnetic coupling between these two layers across the non-magnetic Cu spacer layer, so that also conclusions about micromagnetic mechanisms can be drawn. Epitaxial Co and Ni films on Cu (001) exhibit different magnetic behavior: Whereas Co films are always magnetized in the film plane [19, 20], Ni films show a perpendicular magnetization in an extended thickness range [21–23]. The easy axis of magnetization is phenomenologically described by magnetic anisotropy energies, which are the magnetization direction dependent parts of the free energy. If a Co and a Ni layer are magnetically coupled across a metallic non-magnetic spacer layer, the coupling energy is favor-

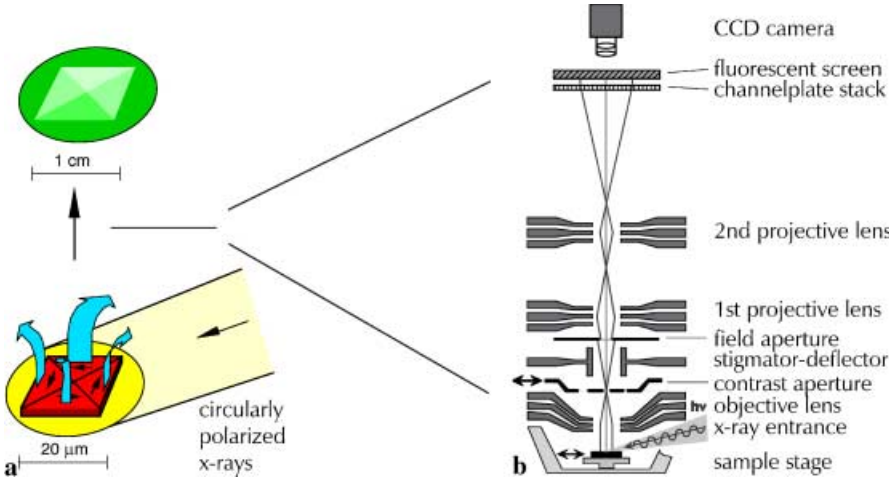

FIGURE 2 Schematic explanation of XMCD magnetic imaging with a PEEM. **a**: Due to XMCD, absorption of a microstructured sample consisting of four magnetic domains is locally different according to the domain structure. This leads to a locally different yield of photo-emitted electrons. A magnified image of the sample created from these electrons displays the magnetic information as intensity differences. **b**: Sketch of the PEEM. Important components are three electrostatic lenses, a contrast aperture to limit the accepted range of electron emission angles, and an image converter consisting of a double multichannel plate and a fluorescent screen

ing a collinear alignment of Co and Ni magnetization directions [24, 25], whereas the anisotropy energies of the magnetic layers are lowest in a non-collinear configuration in which Ni is magnetized out-of-plane, and Co is magnetized in-plane. Spin reorientation transitions between these two configurations can thus be expected if the relative weight of these different energy contributions is varied by varying the layer thicknesses.

2 Experiment

All measurements presented here were performed at the helical undulator beamline UE56-2 of BESSY II in Berlin [26]. Circularly polarized light emitted in the fifth harmonic of the undulator with a degree of polarization of about 80% was used, incident to the sample under an angle of 60° from the surface normal. The helicity of the circular polarization could be changed by shifting part of the magnet structures in the undulator along the beam axis.

Co/Cu/Ni films on Cu (001) were grown and imaged at room temperature in an ultrahigh vacuum chamber (base pressure 1×10^{-8} Pa in the sample preparation chamber, and 2×10^{-8} Pa in the PEEM chamber) equipped with standard facilities for sample preparation and surface characterization. Nickel, copper, and cobalt films were evaporated by electron bombardment from high-purity material. Deposition rates were around 0.5 atomic monolayers (ML) per minute. Film thicknesses were derived from medium energy electron diffraction oscillations during growth and Auger electron spectroscopy. The accuracy of the cited thicknesses is estimated as 10% for Ni and Co, and 20% for Cu. The Co layer was prepared either as a continuous film of a constant thickness, or as a 320 μm wide wedge. Deposition of the latter was achieved by positioning a 2×0.5 mm^2 slit aperture in front of the sample and rocking the sample-mask assembly about the long axis of the aperture during film deposition, as described in more detail in reference [27].

The commercially available PEEM (Focus IS-PEEM) was operated at an accelerating voltage of 12 kV with a contrast aperture of 70 μm diameter, which resulted in a resolution of about 400 nm. The projection lens voltages were adjusted to give a field of view of 60 μm. Images are presented in the form of grayscale coded absorption asymmetry plots for opposite light helicity at the maxima of the Ni and Co L_3 edges, respectively (cf. Fig. 1). The asymmetry is proportional to the cosine of the angle between the local magnetization direction and the light incidence. The images were computer-recorded off a fluorescence screen with 12-bit resolution by a Peltier-cooled camera (PCO SensiCam), which was operated with 2×2 binning of pixels. The acquisition times for the images presented here were 6 min for each helicity.

3 Results and discussion

Figure 3 shows magnetic domain images of a trilayer consisting of a Co wedge on top of four atomic monolayers (ML) Cu/15 ML Ni/Cu (001). The layer sequence is shown schematically at the top of the figure. Layer-resolved domain images of the Ni layer are shown in panels (a) and (c), domain images of the Co layer at the same position are shown in panels (b) and (d). The Co thickness increases in the images from ≈ 1.3 ML at the left to ≈ 2.4 ML at the right of each image, as indicated at the bottom axes. To identify the two angles that define the direction of the magnetization vector in space, two independent measurements are needed. This is achieved by rotating the sample azimuth, which changes the azimuthal direction of the incoming X-rays. The top and bottom images of Fig. 3 are magnetic domain images acquired under two different geometries, with a 170° different light incidence azimuth, as marked by arrows labeled "$h\nu$". From these two measurement geometries it is possible to determine the magnetization vector in space. Since the relative orientation of an out-of-plane magnetization direction and the light incidence does not change under an azimuthal rotation of the light incidence, no change in contrast is expected for out-of-plane domains. For in-plane domains, on the contrary, the relative orientation between the magnetization direction and the light incidence direction

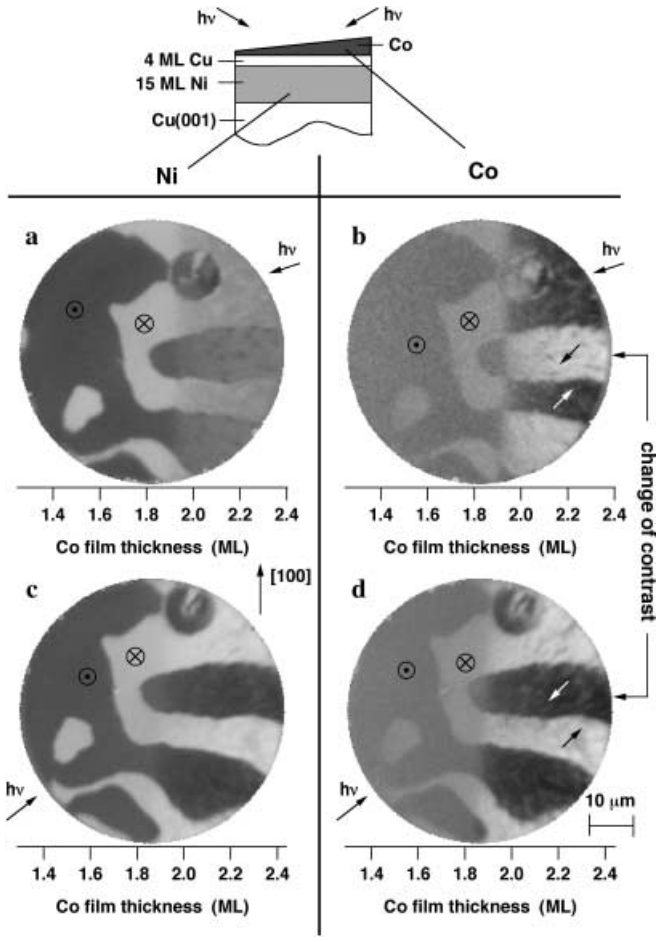

FIGURE 3 Layer-resolved magnetic domain images of a Co wedge on 4 ML Cu/15 ML Ni/Cu (001). The sample is schematically shown at the top. **a**, **c**: Layer-resolved domain images of the Ni layer. **b**, **d**: Layer-resolved domain images of the Co layer. The Co thickness increases in the images from ≈ 1.3 ML to ≈ 2.4 ML, as indicated at the bottom axes. To fully identify the magnetization vector in space, images for two different azimuthal directions of the incoming X-rays, indicated by *arrows* labeled "$h\nu$", have been acquired, and are shown as (**a**), (**b**), and (**c**), (**d**). A reorientation transition between a collinear and a non-collinear magnetic configuration is recognized. On the left hand side both Ni and Co layers are magnetized along out-of-plane directions, whereas on the right hand side the Co magnetization is along $[1\bar{1}0]$ and $[\bar{1}10]$ in-plane directions, as indicated by *arrows*, and Ni is magnetized along canted directions

changes as the azimuth of the exciting X-rays is rotated. For in-plane magnetized domains a contrast reversal is consequently expected for a near-opposite change of the light incidence azimuth.

Comparing the Co images (b) and (d), two regions with different behavior upon light incidence variation are clearly distinguished: Whereas the (weaker) contrast in the left part of the image remains unchanged, the contrast in the right part reverses. We can thus conclude that out-of-plane magnetization is present in the left part of the image, and in-plane magnetization along the $[1\bar{1}0]$ and $[\bar{1}10]$ directions in the right part, as indicated by arrows. In between these two regions a spin-reorientation transition takes place in the Co layer. The circular feature in the images is a macroscopic defect in the substrate, which helped to quickly relocate the same spot on the sample after azimuth rotation.

In the Ni domain images (a) and (c) no contrast reversal as in part of the Co images is observed. However, also here the left and right parts of the images behave differently under azimuth rotation. Like in the Co images, the contrast in the left part of images (a) and (c) is identical. Also the Ni magnetization is out-of-plane in that part of the image, and Ni and Co magnetization directions are thus collinear. Even though the contrast in the right part of the Ni images does not reverse, there is a substantial difference between images (a) and (c): The contrast between bright and dark domains is stronger in (c) than in (a). We can conclude that here neither a pure out-of-plane orientation nor a pure in-plane orientation is present. Quantitative analysis of the grayscale contrast reveals that here the Ni magnetization is canted by about 23° away from the out-of-plane direction into the $[1\bar{1}0]$ and $[\bar{1}10]$ in-plane directions of the corresponding Co domains.

A reorientation transition between a collinear and a non-collinear configuration of the Co/Cu/Ni trilayers is consequently taking place in the middle of Fig. 3 [14]. The collinear configuration has an out-of-plane magnetization. The Ni is magnetized along a canted direction in the non-collinear configuration, whereas the Co magnetization is in the film plane. This canting can be understood considering the competition between the magnetic anisotropies of the Co and Ni layers, and the magnetic interlayer coupling across the Cu spacer layer. Whereas the perpendicular anisotropy of the Ni layer tends to orient Ni out-of-plane, the interlayer coupling tries to align it parallel with the Co moment, thus leading to a canted configuration [15]. For the very low Co thicknesses present in Fig. 3, the Curie temperature of the Co layer is close to room temperature. The magnetic anisotropies are strongly reduced close to the Curie temperature, so that the Co layer is here easily rotated out-of-plane by the interlayer coupling. It is also possible that in the thickness region where the collinear configuration in Fig. 3 is observed, no ferromagnetic order in the Co layer at room temperature would be observed without the magnetic coupling to the Ni layer. Sizable coupling-induced shifts of the ferromagnetic ordering temperature have been indeed observed in Ni/Cu/Co trilayers on Cu (001), although at different thicknesses [28–30]. It is therefore possible that the Co layer on the left hand side of Fig. 3 is below its percolation threshold and consists of weakly coupled paramagnetic islands [31], the room temperature ferromagnetism in which is induced by the coupling to the Ni layer.

The measured secondary electron signal arising from absorption in the Ni layer can be affected by spin-polarized transmission through the ferromagnetic Co top layer [32–34]. The transmission of the spin-polarized secondary electrons created in the ferromagnetic Ni layer through the ferromagnetic Co layer depends on the relative orientation of Ni and Co magnetization directions. Since this orientation is locally constant, this so-called spin filtering effect affects only the total intensity, and cancels out when calculating the asymmetry upon helicity reversal, which only is displayed and analyzed here.

A set of layer-resolved domain images for a slightly higher Cu spacer layer thickness is shown in Fig. 4. Here the sample was 6 ML Co/6 ML Cu/15 ML Ni/Cu (001). Panel (a) on the left hand side shows the layer-resolved domain image of the Ni layer, panel (b) on the right hand side shows the domain image of the Co layer at the same sample position. Only images for one fixed light incidence direction are presented. Measurements under different geometries confirmed that for this Cu spacer layer thickness the magnetization direction in the Ni layer was out-of-plane and the magnetization direction in the Co layer was in-plane, as indicated in Fig. 4. Comparison of the two images reveals two important features. First, much more domains are seen in the Co layer than in the Ni layer. Co domains of three different grayscales, bright, medium dark, and dark, corresponding to $[\bar{1}10]$, $[\bar{1}\bar{1}0]$, and $[1\bar{1}0]$ in-plane magnetization directions, respectively, are observed in a region where Ni displays only one large domain of bright contrast (i.e. magnetization pointing into the film plane along $[00\bar{1}]$). Second, the dark domain in the Ni layer, in which the Ni magnetization is pointing along the [001] surface normal, is reproduced as a dark domain in the Co layer, however, with a $[1\bar{1}0]$ in-plane magnetization.

Although the Co magnetization, from an energetic point of view, does not need to follow the Ni magnetization in this non-collinear magnetization configuration, there is a stunning correspondence in the domain pattern of the out-of-plane

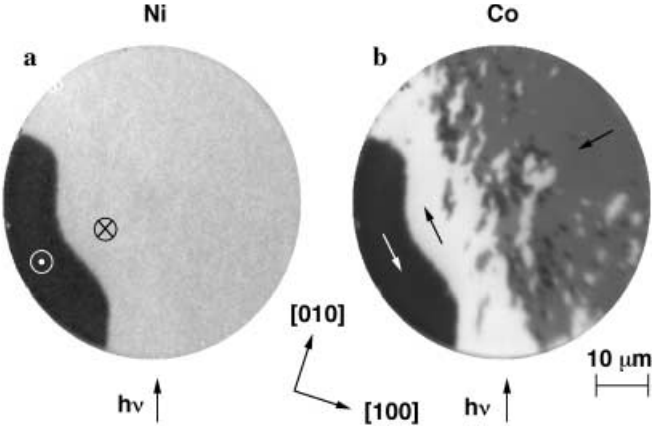

FIGURE 4 Layer-resolved magnetic domain images of 6 ML Co/6 ML Cu/15 ML Ni/Cu (001). **a**: Layer-resolved domain image of the Ni layer. **b**: Layer-resolved domain image of the Co layer. Although the Ni layer is magnetized along the ±[001] out-of-plane directions and the Co layer along ⟨110⟩ in-plane directions, as indicated by *arrows*, a correlation in the domain patterns is observed

magnetized Ni layer and the in-plane magnetized Co layer. In the bottom left part of the images this is the correlation $[001]_{Ni}/[1\bar{1}0]_{Co}$ and $[00\bar{1}]_{Ni}/[\bar{1}10]_{Co}$, which is manifest as dark/dark and white/white correlation in the images. Separated from this region by a stripe with smaller domains in the Co layer is a region on the upper right hand side in which mainly $[00\bar{1}]_{Ni}/[\bar{1}\bar{1}0]_{Co}$ is observed.

The mechanism which is leading to this correlation between Ni out-of-plane and Co in-plane domains on a lengthscale of several ten micrometers is not yet fully clear. From Fig. 3 we know that the Co layer during growth first assumes an out-of-plane magnetization at low thicknesses. In this collinear out-of-plane configuration of the trilayer the domain patterns in both layers are identical (cf. Fig. 3, left part). The final domain pattern as seen in Fig. 4 is likely formed during the subsequent spin-reorientation transition in the Co layer from out-of-plane to in-plane. One hypothesis is that the step orientation of monatomic terraces on the Cu (001) substrate could break the fourfold symmetry and induce such a unidirectional correlation on the observed lengthscales. It has indeed been reported that the in-plane component of Ni films on stepped Cu substrates is perpendicular to the step edges [35].

In Fig. 3 there are actually also some small regions that do not follow this correlation mechanism. They lead to the "cloudy" appearance of the Co domain pattern in the in-plane magnetized region on the right hand side of the Co images (b) and (d). This is due to scattered small domains inside the larger domains with different magnetization directions. Overall, however, the correlation with the Ni domain pattern is clearly visible.

A close inspection of the Co domain wall which correlates with the domain wall in the Ni layer reveals that there is a small but distinct shift in the position of these walls. To illustrate this, in Fig. 5 a difference image between the two images of Fig. 4 is printed. It has been calculated as the Co image (Fig. 4b) minus the Ni image (Fig. 4a), after weighting the images to give identical contrast in the difference image on both sides of the domain wall. A small white stripe is recognized at the position of this wall in Fig. 5. It indicates a region close to the domain wall in which the Co magnetization is along $[\bar{1}10]$ (bright), and the Ni magnetization is along [001] (dark). There is consequently a systematic displacement of the Co domain wall towards the left of the image with respect to the Ni domain wall, to which it seems correlated by shape and approximate position. This displacement varies along the wall between about 200 and 500 nm. Note that a bright stripe with reduced contrast in Fig. 5 indicates a domain wall displacement of less than the instrumental resolution, which was set to 400 nm in the present case.

This effect is getting more pronounced for slightly thinner Cu spacer layers. This is demonstrated in Fig. 6. It shows layer-resolved domain images of a 4 ML Co/4.5 ML Cu/15 ML Ni trilayer on Cu (001). Panel (a) on the left hand side again displays the domain image of the Ni layer, panel (b) on the right hand side the domain image of the Co layer. The domain image of the Ni layer is qualitatively similar to the one of Fig. 4a. The Co image shows again much more and smaller domains than the Ni image, the four different grayscale contrasts of which correspond to magnetization directions along

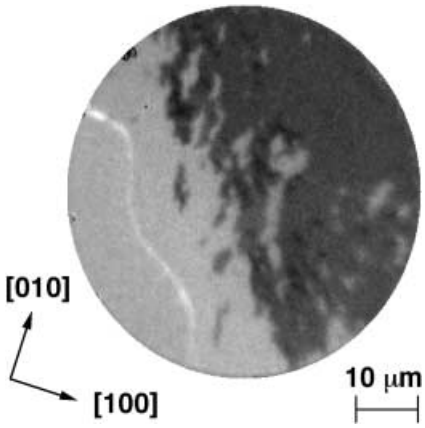

FIGURE 5 Weighted difference between the two images of Fig. 4, calculated as Fig. 4b minus c × Fig. 4a. c was adjusted to give identical contrast on both sides of the domain wall of Fig. 4a. The small white stripe indicates a displacement of the Co domain wall with respect to the Ni domain wall by 200–500 nm towards the left hand side of the image

the four ⟨110⟩ in-plane crystallographic directions, as indicated by arrows in some of the domains. Because of the thinner Cu spacer layer compared to Fig. 4, canting of the Ni magnetization away from the out-of-plane direction is now evident in Fig. 6a from the weak contrast inside the big bright domain. The angle by which the Ni magnetization is canted into the direction of the Co in-plane magnetization amounts to about 6°. Like in Fig. 4, also here the Ni domain pattern is qualitatively reproduced in the Co domain pattern. The dark [001] domain in Ni corresponds to a dark gray $[\bar{1}\bar{1}0]$ domain in Co, and at the adjacent bright $[00\bar{1}]$ domain in Ni predominantly a brighter gray [110] magnetization direction is observed in Co. To compare the positions of the domain walls between these two domains in Ni and Co, a contour line of the Ni domain image, corresponding to the position of 50% contrast change between dark and bright, is overlaid on the Co image (Fig. 6b) as a black line. Clear differences in the positions of the domain walls in the Ni and Co images are recognized. Throughout the image, the position of the domain wall in the Co layer is displaced towards the lower left compared to the Ni domain wall. This displacement varies locally between 400 nm and 2 μm, leading to a more frayed appearance of the wall in Co compared to the straighter line in Ni. The situation is thus qualitatively identical to Fig. 4, where also a displacement of the Co domain wall with respect to the Ni domain wall has been observed.

This displacement of the Co domain walls with respect to the Ni domain walls can be explained by local magnetic stray fields from the Ni domain walls. A sketch explaining the situation is shown in Fig. 7. A domain wall in the Ni layer separates a dark ($+z$-magnetized) domain on the left from a bright ($-z$-magnetized) domain on the right. This causes a magnetic stray field above the domain wall of the Ni film with an in-plane x component pointing to the right, as indicated in the sketch. In addition, there is also a z component of the stray field, which changes sign above the center of the Ni domain wall. The situation in Figs. 4 and 6 is such that the Co layer, at that position, has a dark ($-x$-magnetized) domain on the left hand side, and a bright ($+x$-magnetized) domain on the right hand side. Since the stray field from the

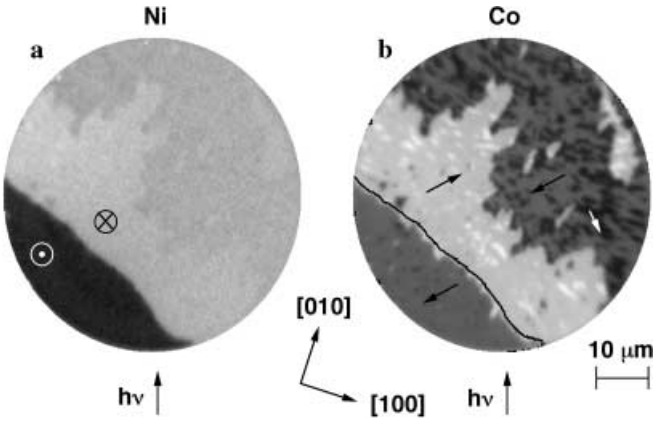

FIGURE 6 Layer-resolved magnetic domain images of 4 ML Co/4.5 ML Cu/15 ML Ni/Cu (001). **a**: Layer-resolved domain image of the Ni layer. **b**: Layer-resolved domain image of the Co layer. The Co layer is magnetized along the four ⟨110⟩ in-plane directions, as indicated by *arrows*, the Ni layer is magnetized along the ±[001] out-of-plane directions with an additional 6° canting away from the film normal into the direction of the Co magnetization. The *black line* in (**b**) is a contour line of the Ni domain image of (**a**), corresponding to the position of 50% contrast change between the two opposite domains. A displacement of the Co domain wall of 0.4–2 μm towards the lower left of the image with respect to the Ni domain wall is recognized

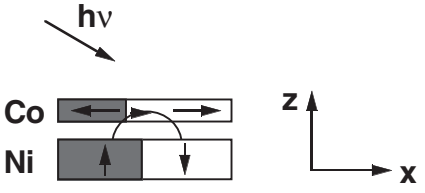

FIGURE 7 Sketch explaining the displacement of the Co domain wall seen in Figs. 4 and 6 by magnetic stray fields from the Ni domain wall. The Ni domain wall causes a magnetic stray field above the Ni layer with an in-plane component pointing to the right. The interaction of this stray field with the Co magnetization causes the observed shift of the position of the Co domain wall to the left, as shown in the sketch

Ni domain wall is pointing to the right, being maximum at the x position of the Ni domain wall, it is energetically favorable if the domain wall in Co is shifted more to the left in order to expand the bright $(+x)$ domain on the expense of the dark $(-x)$ domain. In this way the Zeeman energy of the Co magnetization in the stray field of the Ni domain wall is lowered.

Such a domain wall stray field interaction is of highest technological and fundamental importance. It had been proposed to explain the high degree of antiferromagnetic order found in as-grown weakly coupled multilayers [36], which is irreversibly lost upon magnetization in an external field. The creeping loss of remanent magnetization of the magnetically hard layer in hard/soft spin valves after repeated magnetization cycles of the soft layer [37] has been also attributed to a stray field domain wall interaction [38]. In this case, domain images of the hard layer, a granular CoPtCr film, revealed an oscillatory decay of the remanent magnetization, consistent with micromagnetic models of magnetostatic domain wall interaction [39]. Despite its obvious importance, relatively little work has focused on this interaction up to now. This may be due to the lack of adequate techniques. In contrast to the globally observable magnetic interlayer coupling by electronic indirect exchange [40, 41] and magnetostatic coupling at conformal interface roughness [42], this type of magnetic interlayer coupling by domain wall fringe fields is acting only locally. Its examination in detail requires a microscopic technique with sufficient interface sensitivity and layer resolution. XMCD-PEEM is therefore ideally suited for the study of such micromagnetic coupling mechanisms.

4 Summary

The magnetic interlayer coupling in epitaxial Co/Cu/Ni trilayers on Cu (001) has been studied by layer-resolved magnetic imaging using XMCD-PEEM. Comparison of domain images of the Co and Ni layer for the same sample position reveals that two coupling mechanisms are active on different lengthscales. The first is the globally observable magnetic interlayer coupling of electronic and/or magnetostatic origin. In Co/Cu/Ni/Cu (001) it competes with the magnetic anisotropies of the single ferromagnetic layers Co and Ni, leading to spin-reorientation transitions between collinear and non-collinear magnetic configurations. In the latter a canted Ni magnetization can be observed. The second coupling mechanism is mediated by the magnetic stray fields from domain walls in the perpendicularly magnetized Ni layer. It acts on the Co layer on a local scale. Quantitative investigations of this mechanism by applying external magnetic fields to the trilayers are underway.

ACKNOWLEDGEMENTS The author thanks X. Gao, J. Gilles, and J. Kirschner for collaboration in the experiments presented here, B. Zada for technical assistance, and F. Offi, L.I. Chelaru, K. Fukumoto, M. Kotsugi, R. Hertel, and F. Porrati for stimulating discussions. Help and support by W. Mahler and the BESSY staff during the beamtimes is gratefully acknowledged. This work is supported by the German Minister for Education and Research (BMBF) under Grant Nos. 05-SL8EF19 and 05-KS1EFA6.

REFERENCES

1 C.H. Tsang, R.E. Fontana, Jr., T. Lin, D.E. Heim, B.A. Gurney, M.L. Williams: IBM J. Res. Develop. **42**, 103 (1998)
2 J.-G. Zhu, Y. Zheng, G.A. Prinz: J. Appl. Phys. **87**, 6668 (2000)
3 J.S. Moodera, G. Mathon: J. Magn. Magn. Mater. **200**, 248 (1999), and references therein
4 Y. Ohno, D.K. Young, B. Beschoten, F. Matsukura, H. Ohno, D.D. Awschalom: Nature **402**, 790 (1999)
5 A.T. Hanbicki, B.T. Jonker, G. Itskos, G. Kioseoglou, A. Petrou: Appl. Phys. Lett. **80**, 1240 (2002)
6 E.B. Myers, D.C. Ralph, J.A. Katine, R.N. Louie, R.A. Buhrman: Science **285**, 867 (1999)
7 W. Weber, S. Riesen, H.C. Siegmann: Science **291**, 1015 (2001)
8 G.A. Prinz: Science **282**, 1660 (1998)
9 G.A. Prinz: J. Magn. Magn. Mater. **200**, 57 (1999)
10 S.A. Wolf, D.D. Awschalom, R.A. Buhrman, J.M. Daughton, S. von Molnar, M.L. Roukes, A.Y. Chtchelkanova, D.M. Treger: Science **294**, 1488 (2001)
11 J. Stöhr, Y. Wu, B.D. Hermsmeier, M.G. Samant, G.R. Harp, S. Koranda, D. Dunham, B.P. Tonner: Science **259**, 658 (1993)
12 W. Swiech, G.H. Fecher, C. Ziethen, O. Schmidt, G. Schönhense, K. Grzelakowski, C.M. Schneider, R. Frömter, H.P. Oepen, J. Kirschner: J. Electron Spectrosc. Relat. Phenom. **84**, 171 (1997)
13 W. Kuch, R. Frömter, J. Gilles, D. Hartmann, C. Ziethen, C.M. Schneider, G. Schönhense, W. Swiech, J. Kirschner: Surf. Rev. Lett. **5**, 1241 (1998)
14 W. Kuch, J. Gilles, X. Gao, J. Kirschner: J. Magn. Magn. Mater. **242**–**245**, 1246 (2002)
15 W. Kuch, X. Gao, J. Kirschner: Phys. Rev. B **65**, 064406 (2002)
16 M. Wöhlecke, G. Borstel: Phys. Rev. B **23**, 980 (1981)
17 H. Ebert: Rep. Prog. Phys. **59**, 1665 (1996)
18 G. Schönhense: J. Phys. Cond. Matt. **11**, 9517 (1999)

19 P. Krams, F. Lauks, R.L. Stamps, B. Hillebrands, G. Güntherodt: Phys. Rev. Lett. **69**, 3674 (1992)
20 M. Kowalewski, C.M. Schneider, B. Heinrich: Phys. Rev. B **47**, 8748 (1993)
21 W.L. O'Brien, B.P. Tonner: Phys. Rev. B **49**, 15 370 (1994)
22 B. Schulz, K. Baberschke: Phys. Rev. B **50**, 13 467 (1994)
23 M. Farle, B. Mirwald-Schulz, A.N. Anisimov, W. Platow, K. Baberschke: Phys. Rev. B **55**, 3708 (1997)
24 B. Heinrich, J.A.C. Bland (Ed.): *Ultrathin magnetic structures,* Vol. 2 (Springer, Berlin 1994)
25 M.D. Stiles: J. Magn. Magn. Mater. **200**, 322 (1999), and references therein
26 M.R. Weiss, R. Follath, K.J.S. Sawhney, F. Senf, J. Bahrdt, W. Frentrup, A. Gaupp, S. Sasaki, M. Scheer, H.-C. Mertins, D. Abramsohn, F. Schäfers, W. Kuch, W. Mahler: Nucl. Instr. and Meth. A **467–468**, 449 (2001)
27 W. Kuch, J. Gilles, F. Offi, S.S. Kang, S. Imada, S. Suga, J. Kirschner: J. Electron Spectrosc. Relat. Phenom. **109**, 249 (2000)
28 P. Srivastava, F. Wilhelm, A. Ney, M. Farle, H. Wende, N. Haack, G. Ceballos, K. Baberschke: Phys. Rev. B **58**, 5701 (1998)
29 A. Ney, F. Wilhelm, M. Farle, P. Poulopoulos, P. Srivastava, K. Baberschke: Phys. Rev. B **59**, R3938 (1999)
30 P.J. Jensen, K.H. Bennemann, P. Poulopoulos, M. Farle, F. Wilhelm, K. Baberschke: Phys. Rev. B **60**, R14 994 (1999)
31 P. Poulopoulos, P.J. Jensen, A. Ney, J. Lindner, K. Baberschke: Phys. Rev. B **65**, 064431 (2002)
32 D.P. Pappas, K.-P. Kämper, B.P. Miller, H. Hopster, D.E. Fowler, C.R. Brundle, A.C. Luntz, Z.-X. Shen: Phys. Rev. Lett. **66**, 504 (1991)
33 G. Schönhense, H.C. Siegmann, Ann. Phys. (Leipzig) **2**, 465 (1993)
34 W. Kuch, M.-T. Lin, K. Meinel, C.M. Schneider, J. Noffke, J. Kirschner: Phys. Rev. B **51**, 12 627 (1995)
35 S.S. Dhesi, H.A. Dürr, G. van der Laan: Phys. Rev. B **59**, 8408 (1999)
36 J.A. Borchers, J.A. Dura, J. Unguris, D. Tulchinsky, M.H. Kelley, C.F. Majkrzak, S.Y. Hsu, R. Loloee, J.W.P. Pratt, J. Bass: Phys. Rev. Lett. **82**, 2796 (1999)
37 S. Gider, B.-U. Runge, A.C. Marley, S.S.P. Parkin: Science **281**, 797 (1998)
38 L. Thomas, M.G. Samant, S.S.P. Parkin: Phys. Rev. Lett. **84**, 1816 (2000)
39 L. Thomas, J. Lüning, A. Scholl, F. Nolting, S. Anders, J. Stöhr, S.S.P. Parkin: Phys. Rev. Lett. **84**, 3462 (2000)
40 P. Bruno, C. Chappert: Phys. Rev. Lett. **67**, 1602 (1991)
41 P. Bruno: Phys. Rev. B **52**, 411 (1995)
42 L. Néel: C. R. Hebd. Seances Acad. Sci. **255**, 1676 (1962)